BULLETIN OF THE POLISH ACADEMY OF SCIENCES
TECHNICAL SCIENCES, Vol. 74(1), 2026, Article number: e155890
DOI: 10.24425/bpasts.2025.155890

An assessment of the intensity of extension-bending coupling and its effect on the stability of a thin laminate plate

Monika ZACZYNSKA*, Mehdi BOHLOOLY FOTOVAT, and Zuzanna KALUZNA

Lodz University of Technology, Faculty of Mechanical Engineering, Department of Strength of Materials, Poland

Abstract. The paper presents an investigation to find a method for assessing the intensity of extension-bending mechanical coupling in the behavior of thin plates. The analysis considers thin, simply supported square laminate plates subjected to in-plane compression. Plates with various plies stacking sequences with extension-bending coupling phenomenon were analyzed employing the finite element method software and using a developed closed-formed equation – the analytical method. The coupling intensity was quantified using two dimensionless stiffness reduction coefficients and a nondimensional anisotropic coefficient, known from literature. A reduction in the buckling load for plates with different layer arrangements, observed during nonlinear analysis, was used as a measure of coupling intensity. The results revealed that laminates with high extension-bending coupling intensity could exhibit up to 19% reduction in the buckling load. Additionally, the individual contributions of coupling intensity parameters to this reduction were identified. The validity of the proposed method was further evaluated for plates with different boundary conditions. These findings provide a foundation for predicting the behavior of mechanically coupled laminates without the need for extensive stability analysis.

Keywords: extension-bending mechanical coupling; buckling load; FEM; analytical method; laminate plate; coupling intensity.

1. INTRODUCTION

The topic of thin-walled composite structures has been well-established in the global scientific literature for approximately 20 years [1–6]. These structures have gained significant attention due to their widespread applications in aerospace, automotive, and other industries. Over the past two decades, research into composites has advanced rapidly, leading to numerous technological and theoretical innovations.

However, some major corporations, such as Boeing, have shifted their focus away from the further development of composite materials, often prioritizing alternative technologies or materials. Despite this trend, composites with symmetric ply arrangements remain widely used, mainly due to their ease of manufacturing and predictable mechanical properties. Symmetric configurations are characterized by predictable behavior under operational loads. These stacking sequences are symmetric concerning the mid-layer, resulting in an extension-bending coupling stiffness matrix equal to zero.

The authors aim to investigate a less conventional and more complex category of composites – those with asymmetric ply arrangements. These structures exhibit intriguing and often unexpected properties, including mechanical coupling, which presents both challenges and opportunities for new applications. Although several studies address this phenomenon, particularly those published by York [6–8] and other researchers, it remains an area that requires further exploration.

Expanding this foundation, York [7] defined laminates based on their response to mechanical or thermal loading and identified 24 possible coupling interactions between extension, bending, shear, and twisting. The laminate stacking sequence associated with each particular type of mechanical coupling was defined. In [8], York presented the study on compressed Z-section columns and the benefits of double-ply design. The research showed that with matching bending stiffness and proper selection of laminate configuration, it was possible to increase effective column length, which can result in a transition from local to overall buckling with increased load. In [9], York further demonstrated that the double-ply designs could achieve laminates with comparable strength to standard-ply designs and maximized anisotropy or extension-shear coupling.

In the literature, nonsymmetrical laminates were mainly analyzed in thin-walled columns. Kolakowski and Mania [10] investigated the effect of the extension-bending coupling matrix on the interactive buckling of FGM-FML (functionally graded material – fiber metal laminate) closed- and open-section columns. The authors indicated elements of stiffness matrices that play a considerable role in open-section columns. Teter *et al.* [11] studied the impact of individual elements of an extension-bending coupling submatrix on the load-carrying capacity of thin-walled hybrid columns. The authors noted that an extension-bending coupling submatrix was beneficial for short columns, and listed elements of the submatrix having a crucial impact on critical loads. The effect of the extension-bending coupling matrix can

*e-mail: monika.zaczynska@p.lodz.pl

Manuscript submitted 2025-03-18, revised 2025-08-22, initially accepted for publication 2025-08-26, published in December 2025.

be neglected in long columns, while in mid-length columns, this matrix decreases the load-carrying capacity of the structure. Kubiak *et al.* [12] numerically investigated the effect of couplings on the post-buckling behavior of laminated channel and lipped channel section beams under bending. Beams made from laminates with nonsymmetric layups exhibited lower stiffness compared to those with antisymmetric ones. The buckling and ultimate loading remained unaffected by elements of extension-bending coupling and bending matrices. Teter and Kolakowski [13] proposed an efficient method based on the susceptibility matrix to determine the lowest buckling mode of laminated columns with mechanical couplings, e.g., extension-bending matrix.

A limited number of researchers restricted their study to the analysis of one type of mechanical coupling. The effect of extension-bending mechanical coupling on the delamination failure was investigated by Samborski [14, 15]. Experimental studies were conducted using the end-notched flexure test. Samborski observed that mechanical coupling in laminates resulted in a nonuniform distribution of the strain energy release rate along the delamination front. In [15], an analytical tool was proposed to describe the onset and propagation of the delamination front and its direction in mechanically coupled laminates. Cui and Li studied bending-twisting mechanical coupling in beams [16]. Analytical calculations reveal an improvement in mechanical properties, including rigidity and stability, by applying laminates with a coupled bending matrix. In contrast, Ansari *et al.* [17] investigated the bending-twisting coupling effect on the stability of cylindrical shells under compressive loads and formulated opposing conclusions. Ansari considered several laminate stacking sequences differentiated by the anisotropy parameter [17], proving that bending-twisting anisotropy led to a 25% decrease in the buckling load for the axially supported shells.

Plates with bending-extension coupling under compression loading were studied by Loughlan [18], who used the finite strip method. This investigation focused on altering the degree of coupling by varying the number of plies. It was observed that extension-bending coupling increased as laminate thickness decreased. Falkowicz *et al.* [19, 20] focused on finding the laminate configuration to maximize the bending-twisting coupling. Bohlooly Fotovat and Kubiak [21] presented a study on the non-bifurcation response of a compressed composite plate with the extension-bending coupling matrix.

Several attempts to describe the intensity of mechanical couplings have been made. The bending-twisting coupling intensity parameter and a nondimensional bending stiffness ratio were proposed by Davidson and Schapery [22]. The authors indicated that small values of a nondimensional bending-stiffness ratio occurred in the plate stress state, i.e., especially in orthotropic layers. Nemeth *et al.* [23, 24] introduced other parameters, describing the level of laminate orthotropy or bending-twisting coupling intensity. Kolakowski *et al.* [10] introduced three parameters to describe the level of mechanical coupling of the extension-bending coupling matrix. While a few parameters describing the coupling intensity were proposed, there is limited information about their practical usefulness or the relationship between these parameters. Therefore, analyzing and understanding the impact of individual mechanical coupling on thin-walled laminates is an open problem.

In general, the review of literature indicates that the effect of mechanical coupling on laminates, particularly nonsymmetric arrangements, remains insufficiently explored. The findings of existing research appear to be inconsistent [15, 16].

Present research proposes conducting analytical and numerical investigations to identify the influence of the extension-bending mechanical coupling on the behavior of the thin-walled laminated simply supported plate subjected to uniform compression. Moreover, the research aims to identify parameters that can predict the intensity of extension-bending coupling and its effect on buckling load based on the elements of stiffness matrices. The novelty of this study lies in quantifying the effect of extension-bending coupling on buckling and in proposing a predictive procedure based on stiffness reduction parameters.

2. MECHANICAL COUPLING

According to the classical laminate plate theory (CLPT), the relationship between the in-plane force vector $\boldsymbol{N}$, bending moment vector $\boldsymbol{M}$, and the in-plane strain vector $\boldsymbol{\varepsilon}$ and curvature vector $\boldsymbol{\kappa}$ has the following form [25, 26]:

$$\begin{Bmatrix} N_x \\ N_y \\ N_{xy} \end{Bmatrix} = \begin{bmatrix} A_{11} & A_{12} & A_{16} \\ A_{21} & A_{22} & A_{26} \\ A_{16} & A_{26} & A_{66} \end{bmatrix} \begin{Bmatrix} \varepsilon_x^0 \\ \varepsilon_y^0 \\ \gamma_{xy}^0 \end{Bmatrix} + \begin{bmatrix} B_{11} & B_{12} & B_{16} \\ B_{21} & B_{22} & B_{26} \\ B_{16} & B_{26} & B_{66} \end{bmatrix} \begin{Bmatrix} \kappa_x \\ \kappa_y \\ \kappa_{xy} \end{Bmatrix},$$
$$\begin{Bmatrix} M_x \\ M_y \\ M_{xy} \end{Bmatrix} = \begin{bmatrix} B_{11} & B_{12} & B_{16} \\ B_{21} & B_{22} & B_{26} \\ B_{16} & B_{26} & B_{66} \end{bmatrix} \begin{Bmatrix} \varepsilon_x^0 \\ \varepsilon_y^0 \\ \gamma_{xy}^0 \end{Bmatrix} + \begin{bmatrix} D_{11} & D_{12} & D_{16} \\ D_{21} & D_{22} & D_{26} \\ D_{16} & D_{26} & D_{66} \end{bmatrix} \begin{Bmatrix} \kappa_x \\ \kappa_y \\ \kappa_{xy} \end{Bmatrix}, \tag{1}$$

where $\boldsymbol{A}$, $\boldsymbol{B}$, and $\boldsymbol{D}$ are extension, coupling, and bending stiffness matrices, respectively. All quantities in these equations correspond to the homogenized properties of the laminate.

Elements of the extension stiffness matrix $\boldsymbol{A}$, coupling stiffness matrix $\boldsymbol{B}$, and bending stiffness matrix $\boldsymbol{D}$ are expressed by the following formulas:

$$A_{ij} = \sum_{k=1}^{N} \left(\overline{Q_{ij}}\right)_k (z_k - z_{k-1}), \tag{2}$$

$$B_{ij} = \frac{1}{2} \sum_{k=1}^{N} \left(\overline{Q_{ij}}\right)_k (z_k^2 - z_{k-1}^2), \tag{3}$$

$$D_{ij} = \frac{1}{3} \sum_{k=1}^{N} \left(\overline{Q_{ij}}\right)_k \left(z_k^3 - z_{k-1}^3\right), \tag{4}$$

where Q_{ij} is the transformed reduced stiffness ($i, j = 1, 2, 6$) and z_k is the distance of the k layer to the laminate mid-plane.

In symmetric laminates, the coupling stiffness matrix $\boldsymbol{B}$ equals zero. Thus, in symmetric laminates, only two types of mechanical couplings are possible:

- A_F coupling (in-plane shear-extension coupling) exists when all elements of $\boldsymbol{A}$ matrix are nonzero.
- D_F coupling (out-of-plane bending-twisting coupling) exists when all elements of the $\boldsymbol{D}$ matrix are nonzero.

In nonsymmetric laminates, where the elements of the $\boldsymbol{B}$ matrix are nonzero, five types of coupling are possible [7]:

- B_l coupling (extension-bending coupling) exists when only B_{11} and B_{22} elements of the $\boldsymbol{B}$ matrix are nonzero.
- B_t coupling (extension-twisting and shearing-bending coupling) exists when only B_{16} and B_{26} elements of the $\boldsymbol{B}$ matrix are nonzero.
- B_{lt} coupling (extension-bending, extension-twisting, and shearing-bending coupling) exists when only B_{11}, B_{22}, B_{16}, and B_{26} elements of the $\boldsymbol{B}$ matrix are nonzero.
- B_S coupling (extension-bending, shearing-twisting coupling) exists when only B_{11}, B_{22}, B_{12}, and B_{66} elements of the $\boldsymbol{B}$ matrix are nonzero.
- B_F coupling (extension-bending, shearing-bending, extension-twisting, and shearing-twisting coupling) exists when all elements of the $\boldsymbol{B}$ matrix are nonzero.

In the structure without mechanical couplings, the stiffness matrices have the form:

A_S (simple laminate) exists when A_{16} and A_{26} elements of the $\boldsymbol{A}$ matrix are zero.

B_0 (uncoupled laminate) exists when all elements of the $\boldsymbol{B}$ matrix are zero.

D_S (simple laminate) exists when D_{16} and D_{26} elements of the $\boldsymbol{D}$ matrix are zero.

3. LAMINATE PLATE

A thin square laminate plate with dimensions $100 \times 100 \times 1$ [mm × mm × mm] made of glass fiber reinforced polymer (GFRP), subjected to axial compressive loading, was considered as presented in Fig. 1. The analyzed plate has a variable number of layers n ($2 < n < 16$); the thickness of the individual layer t_l, $t_l = t/n$. It is assumed that the plate is made of unidirectional prepreg material E-glass 1200tex fibers immersed in NTPT THINPREG^{TM} 402 epoxy resin, with nominal properties presented in Table 1. The plates with different stacking sequences were considered. These are presented in Table 2. In the case of fiber orientation in a compressive direction (along the x-axis according to Fig. 1), the angle is equal to 0 degrees.

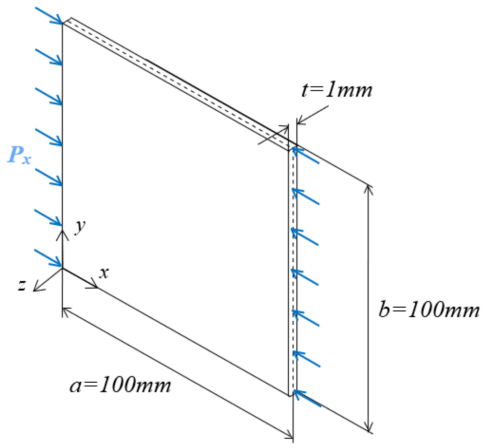

Fig. 1. GFRP plate under consideration

Table 1
Mechanical properties of the composite layers

E_1 [GPa]	E_2 [GPa]	G_{12} [GPa]	G_{23} [GPa]	ν_{12}
30	9.4	9.2	2.7	0.28
UT_f [MPa]	UT_m [MPa]	UC_f [MPa]	UC_m [MPa]	US [MPa]
4260	43	−620	−140	130

Table 2
Considered stacking sequences of plates

No.	ID	Stacking sequence	No. of layers n	Angle α
1.	CP1	[0/90]	2	
2.	CP2	[0/0/90/0]	4	
3.	CP3	[90/0/90/0]	4	
4.	CP4	$[0_7/90_5]^*$	12	
5.	CP5	$[0_7/90/0/90_3]$	12	
6.	CP6	$[0_6/90_5/0]$	12	
7.	CP7	$[0_6/90_2/0/90_2/0]$	12	
8.	CP8	$[0_7/90_3/0_2]$	12	
9.	CP9	$[0_7/90/0/90/0_2]$	12	
10.	CP10	$[0_8/90/0_3]$	12	
11.	CP11	$[0_6/90_2/0_4]$	12	
12.	CP12	$[0_7/90/0_4]$	12	
13.	CP13	$[0_5/90/0/90/0_4]$	12	
14.	CP14	$[0_6/90/0_5]$	12	
15.	S1	$[\alpha/-\alpha/0/-\alpha/0/\alpha/90/\alpha/-\alpha]$	9	(30; 45; 60; 80)
16.	S2	$[-\alpha/\alpha/0/\alpha/0/-\alpha_2/\alpha/-\alpha/\alpha_2/90/-\alpha/90/-\alpha/\alpha]$	16	
17.	S3	$[\alpha/0/-\alpha/0/-\alpha_2/\alpha_2/90/\alpha/90/-\alpha]$	12	

* Numerical subscripts denote the number of layers of the same fiber orientation.

With the variation in layer configuration of the sample (see Table 2), the values of components of the $\boldsymbol{A}$, $\boldsymbol{B}$, and $\boldsymbol{D}$ stiffness matrices differ. Simultaneously, all considered layer arrangements show only extension-bending coupling (denoted as $A_S B_l D_S$). This leads to various effects of extension-bending coupling on

plate behavior, its buckling load, and post-buckling stiffness. Some attempts were made to describe the intensity of mechanical couplings based on the elements of the stiffness matrix. Kolakowski and Mania [10] proposed dimensionless stiffness reduction coefficients (5) and (6) to measure the impact of the coupling matrix $\boldsymbol{B}$ on buckling behavior.

$$\alpha_x = 1 - \frac{B_{11}^2}{A_{11}D_{11}}, \tag{5}$$

$$\alpha_y = 1 - \frac{B_{22}^2}{A_{22}D_{22}}. \tag{6}$$

Based on the preliminary analysis conducted by the authors of this research, it was observed that relying solely on the parameters proposed by Kolakowski [10] was insufficient. To describe the intensity of extension-bending (B_l) coupling in $A_s B_l D_s$ laminates, the parameters α_x, α_y and the nondimensional anisotropic coefficient β should be applied simultaneously. The nondimensional anisotropic coefficient was introduced by Nemeth [23,24] and is defined as

$$\beta = \frac{2(D_{12}+2D_{66})}{\sqrt{D_{11}D_{22}}}. \tag{7}$$

4. METHODS

4.1. Analytical method (AM)

This section presents an analytical formulation for thin-walled composite plates subjected to axial compressive loading. While the formulation follows established theoretical principles [21], its application to determine the nonlinear buckling load in the current context is novel and therefore described in detail. The study is devoted to the thin-walled composite plate subjected to static axial compressive loading. In those structures, the relations between the in-plane force vector $\boldsymbol{N}$, the bending moment vector $\boldsymbol{M}$, and the in-plane strain vector $\boldsymbol{\varepsilon}$ and curvature vector $\boldsymbol{\kappa}$ can be written as

$$\begin{bmatrix} \boldsymbol{\varepsilon}^0 \\ \boldsymbol{M} \end{bmatrix} = \begin{bmatrix} \boldsymbol{A}^* & \boldsymbol{B}^* \\ \boldsymbol{B}^{**} & \boldsymbol{D}^* \end{bmatrix} \begin{bmatrix} \boldsymbol{N} \\ \boldsymbol{\kappa} \end{bmatrix}, \tag{8}$$

and $\boldsymbol{A}^* = \boldsymbol{A}^{-1}$, $\boldsymbol{B}^* = -\boldsymbol{A}^{-1}\boldsymbol{B}$, $\boldsymbol{B}^{**} = \boldsymbol{B}\boldsymbol{A}^{-1}$, and $\boldsymbol{D}^* = \boldsymbol{D} - \boldsymbol{B}\boldsymbol{A}^{-1}\boldsymbol{B}$. On the right side, the force resultants and curvatures can be replaced by two functions, as stress F and deflection w

$$\boldsymbol{N} = \left(F_{,yy}\ F_{,xx} - F_{,xy}\right)^T, \tag{9}$$

$$\boldsymbol{\kappa} = -\left(w_{,xx}\ w_{,yy}\ 2w_{,xy}\right)^T, \tag{10}$$

where a comma means a partial derivative with respect to x and/or y. The compatibility equation of a rectangular plate composed of any arbitrary material is [18]

$$\frac{\partial^2 \varepsilon_x^0}{\partial y^2} + \frac{\partial^2 \varepsilon_y^0}{\partial x^2} - \frac{\partial^2 \varepsilon_{xy}^0}{\partial x \partial y} - \frac{\partial^2 w}{\partial x \partial y} \cdot \frac{\partial^2 w}{\partial x \partial y} + \frac{\partial^2 w}{\partial x^2} \cdot \frac{\partial^2 w}{\partial y^2} + \frac{\partial^2 w}{\partial x^2} \cdot \frac{\partial^2 \breve{w}}{\partial y^2} + \frac{\partial^2 \breve{w}}{\partial x^2} \cdot \frac{\partial^2 w}{\partial y^2} - 2\frac{\partial^2 w}{\partial x \partial y} \cdot \frac{\partial^2 \breve{w}}{\partial x \partial y} = 0. \tag{11}$$

The compatibility equation can be solved by considering a suitable deflection function. Herein, all four edges of the plate are considered movable and simply supported. Then, the approximations of deflection and initial imperfection can be selected in the form of some sinusoidal functions, such as

$$w = f \sin(m_1 x) \sin(n_1 y), \tag{12}$$

$$\breve{w} = g \sin(m_1 x) \sin(n_1 y), \tag{13}$$

where

$m_1 = \dfrac{m\pi}{a}$, where m is the number of half-waves in the x-direction, and a is the plate length;

$n_1 = \dfrac{n\pi}{b}$, where n is the number of half-waves in the y-direction, and b is the plate width;

f is an unknown amplitude of deflection;

g is a known amplitude of geometrical imperfection.

By substituting equations (12) and (13) in (11), the explicit form of the stress function can be derived as

$$F = \psi_1 \cos(2m_1 x) + \psi_2 \cos(2n_1 y) + \psi_3 \sin(m_1 x) \sin(n_1 y) - \frac{1}{2} P_x t y^2, \tag{14}$$

where

$$\psi_1 = \frac{f(f+2g)n_1^2}{32 b_3 m_1^2}, \tag{15}$$

$$\psi_2 = \frac{f(f+2g)m_1^2}{32 b_4 n_1^2}, \tag{16}$$

$$\psi_3 = \frac{-f\left(b_2 m_1^2 n_1^2 - b_5 m_1^4 - b_6 n_1^4\right)}{b_1 m_1^2 n_1^2 + b_3 m_1^4 + b_4 n_1^4}. \tag{17}$$

Coefficients $b_1, b_2, \ldots, b_6$ are listed in Appendix A, and P_x is the compressive force (as presented in Fig. 1).

To obtain the equilibrium equation of the plate, the virtual displacement principle can be applied, where a variation of total potential energy is equal to

$$\int_0^b \int_0^a \left[\frac{\partial^2 M_x}{\partial x^2} + \frac{\partial^2 M_y}{\partial y^2} + 2\frac{\partial^2 M_{xy}}{\partial x \partial y} + N_x \left(\frac{\partial^2 w}{\partial x^2} + \frac{\partial^2 \breve{w}}{\partial x^2} \right) + N_y \left(\frac{\partial^2 w}{\partial y^2} + \frac{\partial^2 \breve{w}}{\partial y^2} \right) + 2N_{xy} \left(\frac{\partial^2 w}{\partial x \partial y} + \frac{\partial^2 \breve{w}}{\partial x \partial y} \right) \right] \delta w \, \mathrm{d}x \, \mathrm{d}y - B_{11}^{**} P_x t \int_0^b \left[\frac{\partial w}{\partial x} \right]_{x=0}^{x=a} \mathrm{d}y - B_{21}^{**} P_x t \int_0^a \left[\frac{\partial w}{\partial y} \right]_{y=0}^{y=b} \mathrm{d}x = 0. \tag{18}$$

By substituting deflection and moment resultants in the above equation, integrating, simplifying, and neglecting small values, the result can be obtained as

$$f+\frac{P_x}{P_{cr}}(f+g+r)+c_1f^3+c_2f^2=0, \tag{19}$$

where

$$P_{cr}=\left(\frac{k_3}{k_2}\right)^{-1},\quad c_1=\frac{k_4}{k_2},\quad c_2=\frac{k_1}{k_2}+\frac{k_5}{k_2},\quad r=\frac{k_6}{k_3}, \tag{20}$$

and the coefficients $k_1, k_2, \ldots, k_6$ are listed in Appendix A. Also, by substitution of equation (14) in (9), the N_x internal force can be found, with dependence on deflection as

$$\begin{aligned}N_x=&\frac{-fm_1^2(f+2g)\cos(2n_1y)}{8b_4}\\&+\frac{f\left(b_2m_1^2n_1^2-b_5m_1^4-b_6n_1^4\right)}{b_1m_1^2n_1^2+b_3m_1^4+b_4n_1^4}\\&\cdot\sin(m_1x)n_1^2\sin(n_1y)-P_xt.\end{aligned} \tag{21}$$

On the other hand, by using the inflection point of equation (21), the deflection of the plate in the nonlinear buckling load can be found as

$$\begin{aligned}&\frac{\mathrm{d}^2}{\mathrm{d}f^2}\left(\frac{P}{P_{cr}}\right)=\frac{\mathrm{d}^2}{\mathrm{d}f^2}\left(\frac{-c_1f^3+c_2f^2+f}{f+g+r}\right)=0\ \Rightarrow\\&f_{nr,cr}=\left[\frac{1}{c_1}\cdot\left(\left(g^3c_1+3g^2c_1r+3gc_1r^2+c_1r^3-g^2c_2\right.\right.\right.\\&\left.\left.\left.-2gc_2r-c_2r^2+g+r\right)c_1^2\right)^{1/3}\right]-g-r,\end{aligned} \tag{22}$$

and $f_{nr,cr}$ is the deflection at the nonlinear buckling load. By employing this deflection to equation (19), the value of the nonlinear buckling load can be found.

The deflection equation for a simply supported laminated plate with extension-bending coupling is presented in equation (19). It is important to note that r represents an extension-bending coupling imperfection [21], which depends on the plate dimensions and elements of the stiffness matrix $\boldsymbol{B}$, while g refers to the amplitude of the initial geometric imperfection. The parameter r, as an artificial coupling imperfection, can be interpreted as an additional geometric imperfection, as it influences the structural behavior in the same way as geometric imperfection g. Thus, when in the considered plate:

- $g=0$ – the equilibrium path that represents the 'pure' effect of extension-bending coupling.
- $r=0$ – the typical equilibrium path for symmetric laminates (without coupling) is obtained.
- $g=-r$ – the typical equilibrium path with a bifurcation point (fork type) is obtained:

$$c_1f^2+c_1f+\frac{P_x}{P_{cr}}+1=0. \tag{23}$$

4.2. Finite element method (FEM)

The finite element method was employed to determine the buckling load using both linear (eigenvalue) and nonlinear analyses. In the present study, a thin square composite plate was modeled using the commercial finite element program ANSYS [27] to predict the buckling behavior of the plates subjected to uniaxial compression. The numerical model, presented in Fig. 2, was created using 400 structural elements SHELL 181 that are four-node elements with six degrees of freedom at each node – three translations (U_X, U_Y, U_Z) and three rotations (ROT_X, ROT_Y, ROT_Z). The model of deformation in chosen elements is based on the first-order shear deformation theory (FSDT). Note that FSDT typically involves only five degrees of freedom (three translations and two rotations). SHELL 181 element supports FSDT by neglecting the in-plane rotational degree of freedom (ROTZ) in the formulation.

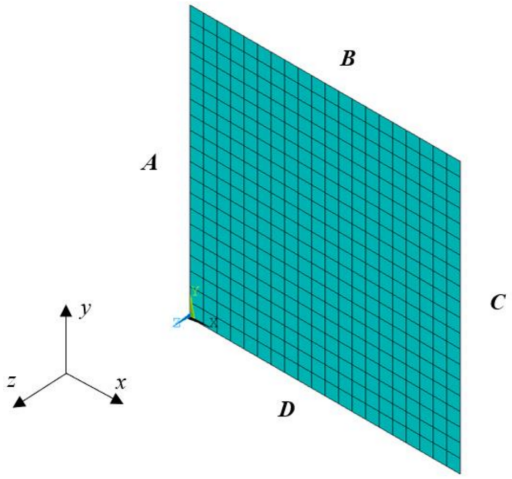

Fig. 2. Discretized FE model

The plate was supported along each edge and subjected to a compressive in-plane load applied along two parallel edges ($x=0$ and $x=a$) – one direction in-plane compression. The influence of mixed boundary conditions on the intensity of mechanical coupling was considered. The plate is simply supported (S) or clamped (C) along the edges parallel to the y-axis, while the other edges can have simply supported (S), clamped (C), or free (F) boundary conditions. Accordingly, the following boundary conditions were considered: SSSS, SSCC, CCFF, CCCC, CCSS, where the first two symbols refer to the loaded edges ($x=0$ and $x=a$), and the last two symbols correspond to the remaining edges ($y=0$ and $y=b$). The boundary conditions considered are summarized in Table 3.

At first, eigenvalue buckling analysis of the simply supported plate was performed using the Block Lanczos method to determine the magnitude of the buckling load and corresponding buckling mode. Then, the independent nonlinear analysis without initial geometric imperfection was performed with the use of the Newton-Raphson algorithm. The results of the linear and nonlinear numerical analysis were compared with the outcomes of an analytical method (AM).

Table 3
Boundary conditions at the edges of the plate

Boundary conditions	*A*	*B*	*C*	*D*
SSSS	$U_X = \text{const.}$; $U_Z = 0$	$U_Y = 0$; $U_Z = 0$	$U_X = 0$; $U_Z = 0$	$U_Y = \text{const.}$; $U_Z = 0$
SSCC	$U_X = \text{const.}$; $U_Z = 0$	$U_Y = 0$; $U_Z = 0$; $ROT_X = 0$	$U_X = 0$; $U_Z = 0$	$U_Y = 0$; $U_X = 0$; $U_Z = 0$; $ROT_X = 0$
CCFF	$U_X = \text{const.}$; $U_Y = 0$; $U_Z = 0$; $ROT_Y = 0$		$U_X = 0$; $U_Y = 0$; $U_Z = 0$; $ROT_Y = 0$	
CCCC	$U_X = \text{const.}$; $U_Z = 0$; $ROT_Y = 0$	$U_Y = 0$; $U_Z = 0$; $ROT_X = 0$	$U_X = 0$; $U_Z = 0$; $ROT_Y = 0$	$U_Y = 0$; $U_Z = 0$; $ROT_X = 0$
CCSS	$U_X = \text{const.}$; $U_Y = 0$; $U_Z = 0$; $ROT_Y = 0$	$U_Y = 0$; $U_Z = 0$	$U_X = 0$; $U_Y = 0$; $U_Z = 0$; $ROT_Y = 0$	$U_Y = \text{const.}$; $U_Z = 0$

5. RESULTS

5.1. Simply supported boundary conditions

The nonlinear buckling analysis, without initial geometric imperfections, was performed using the Newton-Raphson algorithm in FEM computations and an analytical method based on (19). Analyzing a perfect plate without any structural imperfections allows for the distinction of the effect of extension-bending coupling on the plate response. Graphs of equilibrium paths were tracked in dimensionless form for all analyzed samples, as presented in Fig. 3. They show the ratio of axial load to the critical buckling load obtained from eigenvalue solution (P/P_{crLBA}) as a function of deflection in the plate center to its thickness (w/t). It can be noticed that the behavior of the plate under compressive loading differs significantly depending on the layer arrangements. For sample CP14, the loss of stability

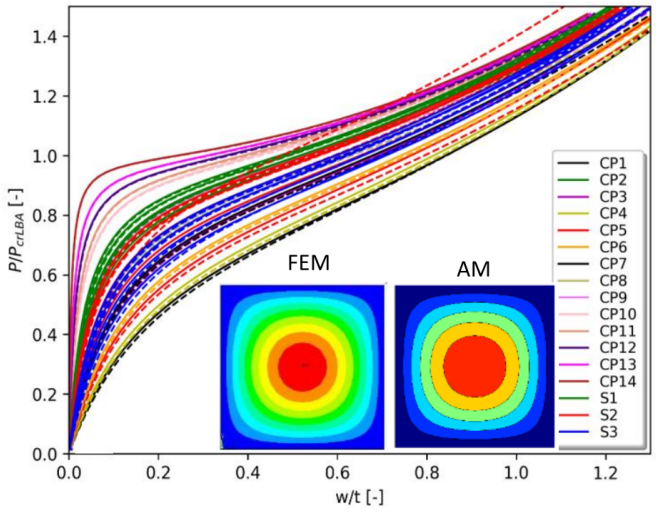

Fig. 3. Dimensionless equilibrium paths of SSSS plates

is observed under load near the eigenvalue solution, while for sample CP1, the plate starts to bend from the very beginning of load application. It should be mentioned that despite the variety in the equilibrium paths, each stacking sequence exhibits the same buckling mode – one half-wave, as presented in Fig. 3.

In the analyzed laminates, bending-extension mechanical coupling causes plate bending from the onset of load application, complicating the determination of the buckling load based on the equilibrium path. Consequently, approximation methods are necessary to estimate the buckling load based on the load-deflection relation. In this study, the inflection point method was employed to estimate critical forces [28]. This method provides an efficient means of estimating the buckling load based on the force-deflection curve and gives consistent results, aligning with the slope reduction in the force-shortening curve [29]. The buckling load is defined as the load at which the second derivative of deflection with respect to load equals zero, $\mathrm{d}^2\left(\frac{w}{t}\right)/\mathrm{d}\left(\frac{P}{P_{crLBA}}\right)^2 = 0$.

Table 4 presents the nondimensional coupling intensity parameters (5)–(7) along with analytical and numerical results: the critical buckling load obtained from linear buckling analysis (P_{crLBA}) and the nondimensional critical buckling load ($P_{crN} = P_{crNLA}/P_{crLBA}$) derived from nonlinear analysis. Additionally, the magnitude of artificial imperfection r/t is listed for each considered stacking sequence. The analytical and numerical results show excellent agreement, with the discrepancy not exceeding 4%. It is also noted that the critical buckling load obtained from eigenvalue analysis (P_{crLBA}) is nearly the sameacross the considered lay-ups. The difference in bifurcation load does not exceed 9% for FEM and 14% for the analytical method, with these differences being primarily observed in cross-ply laminates (CP1–CP14). Standard-angle ply laminates (S1–S3) exhibit nearly identical buckling loads, with discrepancies of less than 3%.

The nondimensional critical buckling load P_{crN} demonstrates the influence of extension-bending coupling, where an increase in coupling intensity results in a greater reduction in the buckling load. Coupling intensity can be assessed in two ways: by analyzing the artificial imperfection r/t or by examining the parameters of α_x, α_y and β. In the first approach, an increase in the parameter r/t indicates an increase in coupling intensity, while in the second approach, the opposite trend is observed. Figure 4a presents the relationship between the artificial imperfection parameter and the decrease in buckling load. Based on the results, it can be observed that the r/t parameter provides a rough estimation of coupling intensity. A general trend of decreasing nondimensional buckling load with increasing r/t is evident, although some regions deviate from this trend (as an example, $P_{crN} = 0.96$ for a range of $r/t = 0.054$–0.082, whereas for sample S1(80), $r/t = 0.064$ with $P_{crN} = 0.97$). In Table 4, the dimensionless buckling load is also presented in relation to dimensionless stiffness reduction coefficients α_x. Here as well, a rough estimation of coupling intensity can be made based on the α_x parameter. While $\alpha_x = 1$, there is no coupling, and thus the dimensionless buckling load should theoretically be equal to

Table 4
Coupling intensity parameters and dimensionless buckling load of the considered lay-ups

					P_{crLBA} [N]		P_{crN} [–]	
ID	α_x	α_y	β	r/t	FEM	AM	FEM	AM
CP1	0.80	0.80	2.09	0.245	622.2	600.7	0.81	0.82
CP2	0.99	0.97	2.35	0.051	673.9	674.2	0.98	0.97
CP3	0.95	0.95	2.09	-0.122	663.5	659.6	0.93	0.92
CP4	0.82	0.79	2.09	0.221	623.6	604.6	0.83	0.83
CP5	0.88	0.82	2.09	0.178	636.0	623.7	0.87	0.86
CP6	0.93	0.86	2.14	0.158	649.2	641.2	0.89	0.89
CP7	0.96	0.90	2.16	0.119	658.8	654.6	0.92	0.92
CP8	0.98	0.92	2.25	0.084	666.4	665.1	0.95	0.94
CP9	0.99	0.96	2.30	0.054	672.6	672.8	0.97	0.96
CP10	1.00	0.99	2.38	0.026	676.7	677.6	0.99	0.98
CP11	1.00	0.99	2.42	0.021	677.3	678.2	0.99	0.99
CP12	1.00	1.00	2.42	0.016	677.7	678.7	1.00	0.99
CP13	1.00	1.00	2.42	0.011	678.0	679.0	1.00	1.00
CP14	1.00	1.00	2.45	0.005	678.2	679.2	1.00	1.00
S1(30)	1.00	0.99	2.03	0.040	666.3	666.6	0.98	0.98
S1(45)	0.99	0.99	1.94	0.044	663.3	663.5	0.98	0.98
S1(60)	0.99	0.99	2.02	0.053	666.6	666.6	0.97	0.97
S1(80)	0.98	1.00	2.29	0.064	674.8	674.6	0.96	0.97
S2(30)	0.99	0.98	2.03	0.057	665.1	664.7	0.97	0.96
S2(45)	0.98	0.98	1.96	0.066	662.8	662.1	0.96	0.96
S2(60)	0.98	0.99	2.21	0.082	665.8	664.7	0.95	0.96
S2(80)	0.96	0.99	2.23	0.105	673.1	671.3	0.93	0.95
S3(30)	0.98	0.96	2.03	0.081	662.2	660.5	0.95	0.95
S3(45)	0.97	0.97	1.98	0.092	660.6	658.4	0.95	0.94
S3(60)	0.96	0.98	2.03	0.110	663.3	660.5	0.92	0.94
S3(80)	0.93	0.98	2.18	0.137	669.6	665.6	0.91	0.92

one. However, preliminary research indicated that all three parameters should be applied simultaneously to accurately assess extension-bending coupling intensity.

To evaluate the influence of the coupling intensity parameters α_x, α_y and the orthotropy parameter β on the dimensionless buckling load P_{crN}, a series of numerical analyses was conducted. For this purpose, selected elements of the extension matrix $\boldsymbol{A}$, the extension bending matrix $\boldsymbol{B}$, and the bending matrix $\boldsymbol{D}$ were modified to obtain specific values of α_x, α_y, and β parameters. The parameter ranges were chosen based on the values typical for $A_S B_l D_S$ coupled laminates (Table 4). When coupling does not occur or has no effect, $P_{crN} = 1.00$. As mechanical coupling increases, the dimensionless buckling load decreases, indicating a reduction in structural stability.

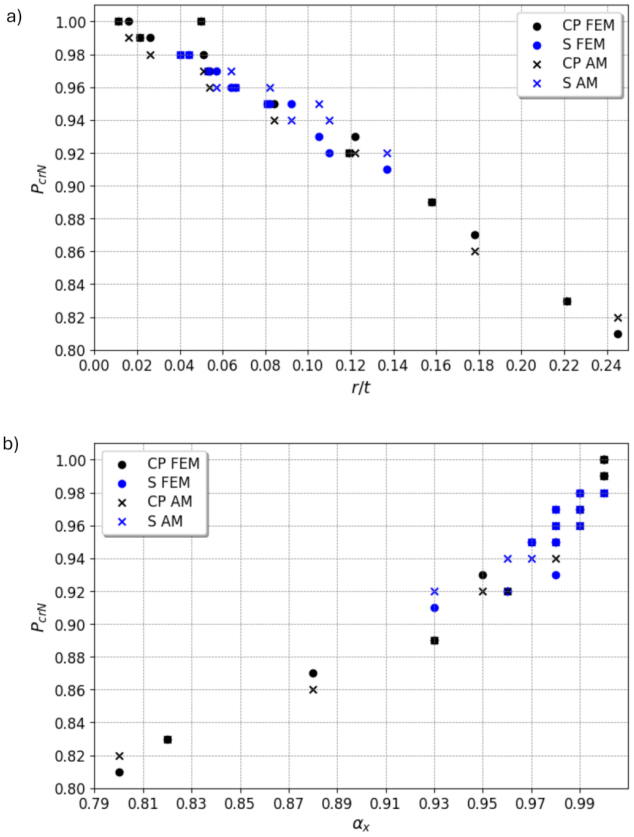

Fig. 4. Dimensionless buckling load in relation to a) r/t parameter, b) stiffness reduction coefficient α_x

The numerical calculations were conducted in two steps:

- Variation of coupling intensity parameters: The coupling intensity parameters α_x and α_y varied independently from 0.79 to 1.00 in increments of 0.02, while the orthotropy parameter β was held constant at 2.089.
- Variation of the orthotropy parameter: The orthotropy parameter β was varied from 1.90 to 2.50 in increments of 0.05. Simultaneously, α_x and α_y varied from 0.79 to 1.00 in increments of 0.02, with the assumption that $\alpha_x = \alpha_y$. Additionally, more detailed analyses were conducted to investigate the effect of the orthotropy parameter for laminates with different α_x and α_y.

Therefore, four additional sets of analyses were conducted for varying β and for the following values of intensity parameters conditions:

- $\alpha_x = 0.79$, $0.79 < \alpha_y < 1.00$
- $\alpha_x = 1.00$, $0.79 < \alpha_y < 1.00$
- $\alpha_y = 0.79$, $0.79 < \alpha_x < 1.00$
- $\alpha_y = 1.00$, $0.79 < \alpha_x < 1.00$

Figure 5 compares the dimensionless buckling load P_{crN} of the plate across different coupling parameters α_x and α_y. In Figs. 5b and 5c, the buckling load values for extreme parameters α_x and α_y are presented. Similarly, Fig. 6 illustrates the effect of the orthotropy parameter for various α_x and α_y.

The results show that the dimensionless buckling load varies between 0.82 and 1.00, depending on the selected parameter values. The percentage change in the dimensionless buckling

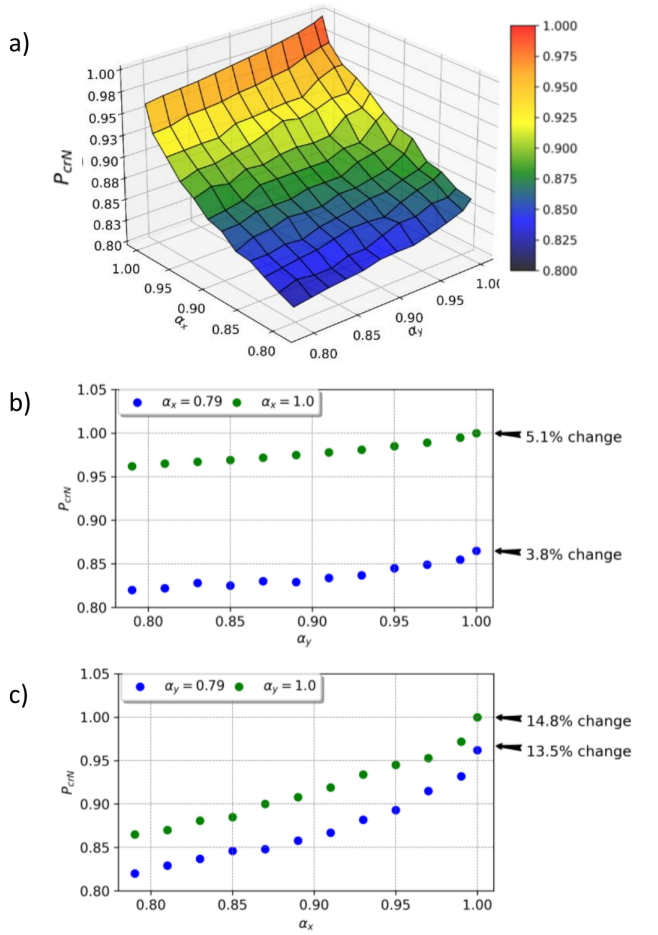

Fig. 5. Influence of the coupling intensity parameters α_x and α_y on the dimensionless buckling load, a) both α_x and α_y varying, b) $\alpha_x = 0.79$ or $\alpha_x = 1.00$, c) $\alpha_y = 0.79$ or $\alpha_y = 1.00$

load was calculated using the following formula:

$$\left[\left(P_{crN}^{\max} - P_{crN}^{\min}\right) / P_{crN}^{\max}\right] \cdot 100\%, \tag{24}$$

where $P_{crN}^{\max}$ and $P_{crN}^{\min}$ is the maximum and minimum dimensionless buckling load, respectively. Among the parameters studied, α_x has the most significant impact, potentially reducing the buckling load up to 14.8%. In contrast, α_y has a smaller influence, causing a reduction of up to 5.1%. The effect of the orthotropy parameter β is minimal, with reductions up to 1.7%. It is noteworthy that β does not directly describe any type of coupling. When $\alpha_x = \alpha_y = 1$, indicating no coupling, the orthotropy parameter does not affect the plate behavior, as evidenced by a constant $P_{crN} = 1.00$ across all β values. However, as the coupling intensity parameters decrease (indicating increased coupling), the influence of the β becomes more pronounced. Thus, while β does not explicitly define coupling effects, it slightly enhances the coupling effect in coupled structures.

The effect of extension-bending mechanical coupling on the distribution of the N_x internal force component was also analyzed using FEM and AM. The internal force N_x was evaluated along half of the half-wavelength of the plate. The distribution of

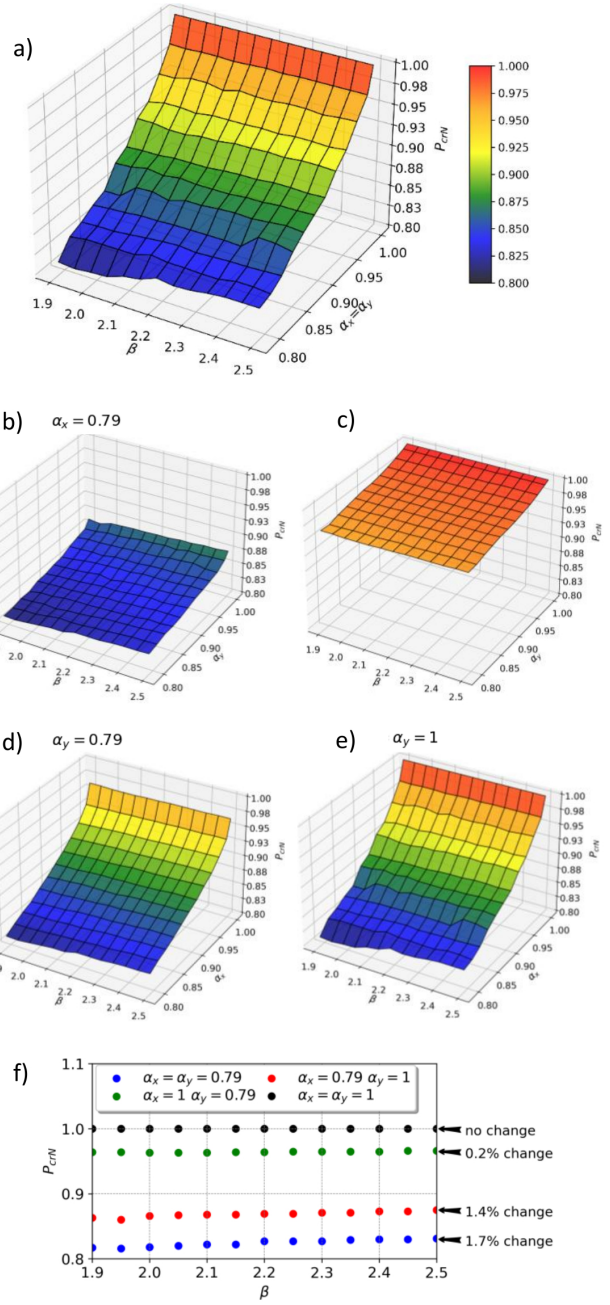

Fig. 6. Influence of the orthotropy parameter β on the dimensionless buckling load P_{crN}: a) $\alpha_x = \alpha_y$, b) $\alpha_x = 0.79$, c) $\alpha_x = 1.00$, d) $\alpha_y = 0.79$, e) $\alpha_y = 1.00$, f) results for extreme values of α_x and α_y

this force across the plate's cross-section is presented in Fig. 7 in dimensionless form, using the parameter "relative internal force" [30]. This parameter is defined as the ratio of a given internal force to the maximum value of the N_x force – $N_{x\max}$.

The analysis examines the variation in the internal force distribution across the pre-buckling (for $P = 0.8P_{crN}$), buckling (for $P = 1.0P_{crN}$), and post-buckling (for $P = 1.2P_{crN}$) regimes for two exemplary lay-ups, CP1 and CP14, which represent the extreme values of the parameter α_x. A comparison of analytical and numerical results shows an elevated level of agreement for the CP14 lay-up, while some discrepancies are observed for the

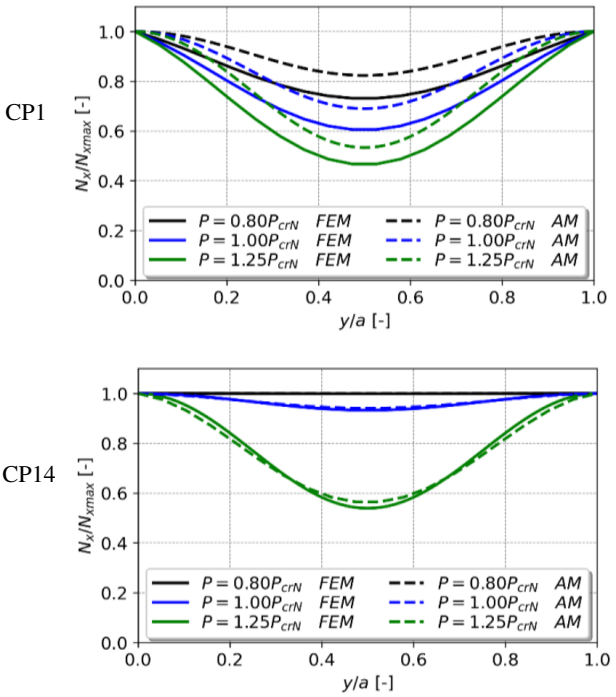

Fig. 7. Distribution of internal force N_x for a) CP1 and b) CP14 lay-ups

CP1 layer arrangement. These discrepancies are attributed to differences in degrees of freedom between the analytical and numerical models. In the case of the analytical method, the sine deflection function was assumed, while in FEM, the deflection function is a result of nodal displacements. In the case of FEM 20, nodes along one line were set, and the chosen element has a linear displacement function. As the CP1 sample exhibits greater deformations due to higher coupling intensity, the differences between the two methods are also more pronounced.

For the CP14 lay-up, which exhibits minimal bending-extension coupling intensity, the analysis reveals that the structure experiences pure compression in the pre-buckling regime. The N_x internal force distribution is uniform across the plate cross-section. However, as the load increases, for $P = P_{crN}$, and subsequently in the post-buckling regime, a nonuniform distribution of the N_x force emerges. This change is attributed to the development of half-wavelength, significantly altering the internal force distribution across the plate width.

In contrast, for lay-ups with high coupling intensity, such as CP1, the situation differs markedly. Even in the pre-buckling regime, a nonuniform distribution of the internal forces is observed. This nonuniformity is indicative of plate bending from the onset of load application and provides unambiguous evidence of extension-bending coupling (compared with Fig. 3). As the load increases to $P = P_{crN}$ and further to $P = 1.25P_{crN}$, this effect becomes more pronounced, with the internal force distribution continuing to evolve significantly.

5.2. Effect of boundary conditions

The coupling intensity on the simply supported plate was evaluated. In the next step, the applicability of the proposed approach was examined for plates with various boundary conditions using the finite element method. To achieve this, several different boundary conditions were considered: CCFF, SSCC, CCCC, and CCSS, where F denotes free, S – simply support, and C – clamped boundary conditions. For example, the notation CCFF refers to a configuration where the two edges parallel to the y-axis are clamped, while the two edges parallel to the x-axis are free.

In Fig. 8, the lowest buckling mode for the exemplary CP1 lay-up and various boundary conditions is presented. It should be noted that, for almost all analyzed cases, the same buckling mode shape was obtained across all analyzed layer arrangements. However, a few exceptions were identified – for SSCC lay-ups S1(45), S1(60), S1(80), S2(45), S2(60), S2(80), S3(45), S3(60), S3(80), while for CCCC lay-ups S1(80), S2(80) and S3(80), as denoted in Table 5 by upper index ($m = 2$). In these exceptions, two half-waves in the longitudinal direction were observed.

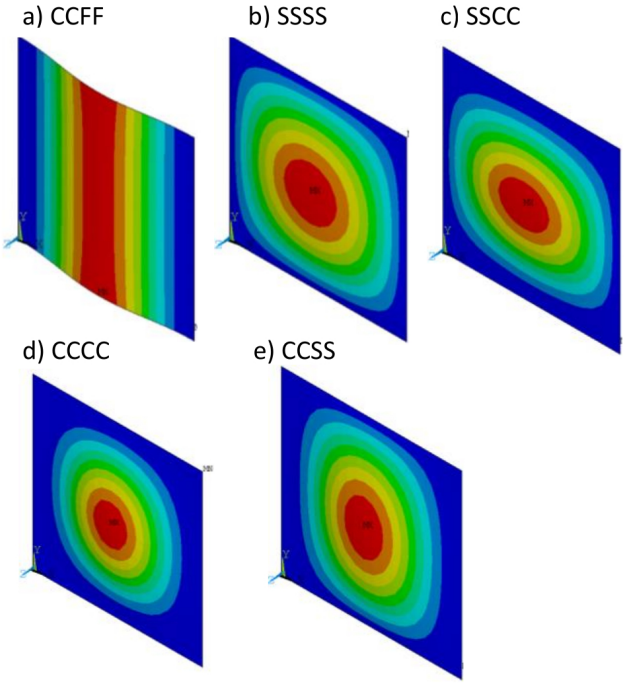

Fig. 8. Buckling mode for sample CP1 for various boundary conditions

Table 5 and Fig. 9 present the critical buckling load (P_{crLBA}) and the dimensionless buckling load (P_{crN}) for the considered lay-ups and boundary conditions. It can be observed that boundary conditions significantly influence the behavior of laminates with extension-bending mechanical coupling. For simply supported boundary conditions, the difference in the critical load (P_{crLBA}) across all considered layer arrangements does not exceed 9%. In contrast, for CCFF boundary conditions, this difference is nearly 270% (lay-up S1(80) compared to CP14).

The effect of boundary conditions is also evident in the dimensionless buckling load (Fig. 9). For CCFF boundary conditions, the effect of extension-bending mechanical coupling is negligible ($P_{crN} = 0.99$ for all considered lay-ups). Conversely, for CCCC and CCSS boundary conditions, no reduction in the

Table 5
Dimensionless buckling load for various boundary conditions

	CCFF		SSSS		SSCC		CCCC		CCSS	
ID	P_{crLBA} [N]	P_{crN} [–]	P_{crLBA} [N]	P_{crN} [–]	P_{crLBA} [N]	P_{crN} [–]	P_{crLBA} [N]	P_{crN} [–]	P_{crLBA} [N]	P_{crN} [–]
CP1	533.9	0.99	622.2	0.81	1094	0.86	1434	1.00	912.5	1.00
CP2	972.7	0.99	673.9	0.98	992.4	0.98	1729	1.00	1286	1.00
CP3	637.6	0.99	663.5	0.93	1212	0.94	1641	1.00	1009	1.00
CP4	553.8	0.99	623.6	0.83	1102	0.90	1450	1.00	936.2	1.00
CP5	623.4	0.99	636.0	0.87	1118	0.93	1523	1.00	1001	1.00
CP6	759.0	0.99	649.2	0.89	1049	0.91	1599	1.00	1101	1.00
CP7	815.1	0.99	658.8	0.92	1056	0.96	1698	1.00	1155	1.00
CP8	902.4	0.99	666.4	0.95	1023	0.97	1692	1.00	1231	1.00
CP9	944.7	0.99	672.6	0.97	1020	0.99	1722	1.00	1272	1.00
CP10	991.6	0.99	676.7	0.99	1002	1.00	1743	1.00	1311	1.00
CP11	1009	0.99	677.3	0.99	981	1.00	1746	1.00	1322	1.00
CP12	1012	0.99	677.7	1.00	987	1.00	1748	1.00	1330	1.00
CP13	1010	0.99	678.0	1.00	983	1.00	1748	1.00	1323	1.00
CP14	1022	0.99	678.2	1.00	979	1.00	1750	1.00	1338	1.00
S1(30)	830.9	0.99	666.3	0.98	1148	0.99	1726	1.00	1176	1.00
S1(45)	681.4	0.99	663.3	0.98	1251 ($m = 2$)	1.00	1703	1.00	1050	1.00
S1(60)	524.9	0.99	666.6	0.97	**1144** ($m = 2$)	**1.17**	1656	1.00	919.6	1.00
S1(80)	381.2	0.99	674.8	0.96	**1048** ($m = 2$)	**1.09**	1454 ($m = 2$)	1.00	797.0	1.00
S2(30)	804.2	0.99	665.1	0.97	1158	0.98	1712	1.00	1155	1.00
S2(45)	673.3	0.99	662.8	0.96	1244	0.98	1692	1.00	1041	1.00
S2(60)	535.6	0.99	665.8	0.95	**1148** ($m = 2$)	**1.11**	1652	1.00	919.5	1.00
S2(80)	408.2	0.99	673.1	0.93	**1056** ($m = 2$)	**1.11**	1500 ($m = 2$)	1.00	800.7	1.00
S3(30)	773.0	0.99	662.2	0.95	1160	0.97	1689	1.00	1284	1.00
S3(45)	661.6	0.99	660.6	0.95	1233	0.97	1672	1.00	1031	1.00
S3(60)	543.8	0.99	663.3	0.92	**1151** ($m = 2$)	**1.07**	1639	1.00	926.2	1.00
S3(80)	434.0	0.99	669.6	0.91	**1073** ($m = 2$)	**1.07**	1541 ($m = 2$)	1.00	823.8	1.00

buckling load due to coupling is observed ($P_{crN} = 1.00$). This suggests that extension-bending mechanical coupling is effectively eliminated when the loaded edge is clamped. A similar observation was reported by Bohlooly-Fotovat and Kubiak [21] for plates clamped along all edges.

Another conclusion can be drawn for plates with simply supported loaded edges and clamped perpendicular edges (SSCC). In this case, for cross-ply laminates (CP1–CP14), the effect of extension-bending coupling is slightly lower than for plates simply supported on all edges. However, the overall trend remains unchanged: clamped boundary conditions at nonloaded edges slightly reduce the effect of coupling compared to SSSS boundary conditions.

The results differ significantly for standard laminates (S1–S3). Surprisingly, for a few-layer arrangement, an increase in the buckling load was observed ($P_{crN} > 1$). These lay-ups are highlighted in bold in Table 5. This increase in buckling load appears to occur for plates with two half-waves in the longi-

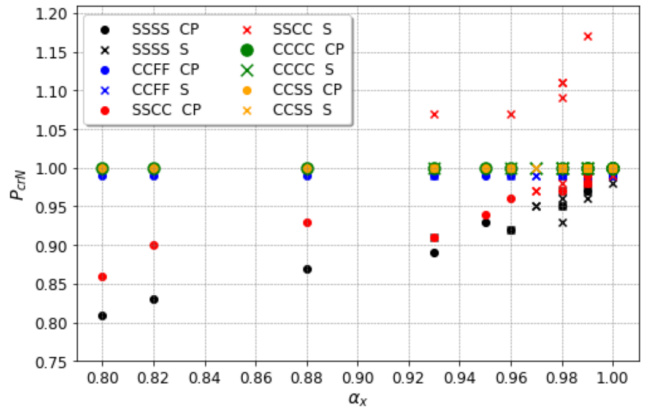

Fig. 9. The effect of the boundary conditions on the dimensionless buckling mode

tudinal direction ($m = 2$). However, for sample S1(45), where $m = 2$, the dimensionless buckling load does not exceed one. To investigate this phenomenon, the equilibrium paths and the relationship between the buckling load and plate length for two samples, S1(45) and S1(60), under SSCC boundary conditions are presented in Fig. 10.

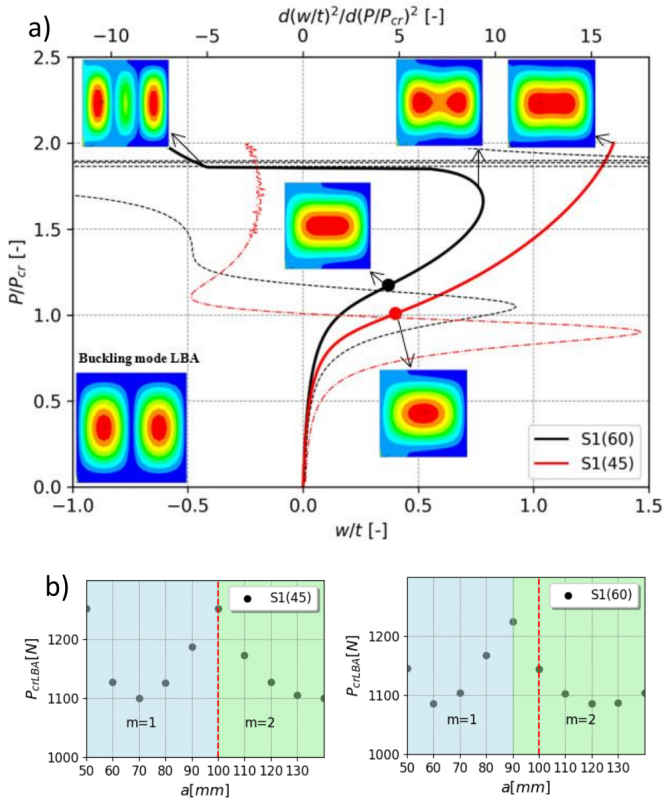

Fig. 10. a) Equilibrium path for S1(45) and S1(60) lay-up and b) buckling force versus length of the plate

Both samples exhibit a buckling mode with two half-waves in the longitudinal direction based on linear buckling analysis (LBA). The dimensionless buckling load P_{crN} was determined from nonlinear analysis without initial geometrical imperfections. P_{crN} was defined based on the second derivative w/t with respect to P/P_{crLBA} (denoted by the dotted line in Fig. 10). The critical point corresponds to the point where this derivative equals zero (denoted by points on the equilibrium path).

Comparing the buckling modes for the nondimensional critical buckling load, one half-wave in the longitudinal direction is observed for both layer arrangements in the nonlinear analysis. In contrast, LBA predicts two half-waves for both layer arrangements. The appearance of two half-waves in the lowest buckling mode from the LBA analysis results from the layer arrangement and the applied boundary conditions. Conversely, in the nonlinear analysis, one half-wave is observed for $P = P_{crN}$ because of extension-bending coupling, which induces plate bending from the beginning of load application. With an increase in load, the number of half-waves does not change for the S1(45) sample, while for S1(60), it transitions to two and three half-waves.

When comparing the buckling force vs. plate length diagrams (Fig. 10b), it is evident that for the S1(45) lay-up at a plate length $a = 100$ mm, the structure is at a transition point between one and two half-waves. Thus, a tendency to develop one half-wave is more pronounced. For the S1(60) lay-up at the same plate length, the structure accommodates two half-waves under compressive loading, leading to a higher resistance for the S1(60) lay-up compared to the S1(45).

6. CONCLUSIONS

The study analyzes the behavior of square GFRP (glass fiber-reinforced polymer) plates with extension-bending coupling under axial compressive loading. Fourteen different cross-ply laminates and three standard laminates with varying fiber orientations were examined. Additionally, a parametric analysis with varied selected elements of $\boldsymbol{A}$, $\boldsymbol{B}$ and $\boldsymbol{D}$ stiffness matrices was performed to explore a broader range of layer arrangements. This enabled the identification of mechanisms influencing the buckling behavior of the coupled plates. The assessment focused on measuring the coupling intensity, its impact on the reduction of buckling load, and the contributions of individual parameters to this reduction. Dimensionless buckling force, defined using the inflection point method, was used as the primary measure. Based on the analysis, the following conclusions were drawn:

- Extension-bending mechanical coupling causes the plate to bend from the onset of loading. Depending on the coupling intensity, the buckling load can be reduced by up to 19%.
- Two dimensionless stiffness reduction coefficients α_x and α_y, and a nondimensional anisotropic coefficient β, are essential for describing coupling intensity in $A_S B_l D_S$ laminates based on the elements of $\boldsymbol{A}$, $\boldsymbol{B}$, and $\boldsymbol{D}$ matrices for square, simply supported plates. Among these coefficients, α_x has the most significant impact on buckling load, potentially reducing it up to 14.8%, while α_y can lead to a 5.1% reduction. The anisotropic coefficient β has a negligible effect on buckling behavior, although it slightly enhances the coupling effect in coupled laminates.
- The artificial imperfection parameter r/t, derived from the analytical method (20) provides only a rough estimation of the coupling intensity.

- Coupling intensity can be observed in the distribution of N_x internal force. Laminates with low coupling intensity show a uniform distribution of internal force in the pre-buckling range. In contrast, high coupling intensity laminates (as C1 lay-up) exhibit nonuniform N_x force distribution even in the pre-buckling stage. This nonuniformity becomes more pronounced as the load increases.
- Boundary conditions significantly influence the response of mechanically coupled laminates. Plates with clamped loaded edges exhibit no extension-bending coupling. For SSCC boundary conditions, cross-ply laminates show slightly less coupling effect than under SSSS conditions. However, standard laminates (S1–S3) exhibit inconsistent trends. In some cases, the development of two half-waves results in an unexpected increase in the buckling load.

The findings contribute to a deeper understanding of the stability of thin-walled composite structures with extension-bending mechanical coupling. A new method for quantifying the intensity of extension-bending coupling in simply supported plates was proposed, providing a practical approach to evaluate and predict the influence of coupling on structural stability. The proposed methodology is applicable to other composite laminates, such as CFRP (carbon fiber reinforced polymer), but the results may vary due to differences in material anisotropy. In particular, variations in the ratio of longitudinal to transverse stiffness may affect the values of coupling intensity parameters and the resulting decrease in buckling load. Interestingly, for a few samples with standard layer orientation under SSCC boundary conditions, an increase in buckling load was observed. This suggests that the presence of extension-bending mechanical coupling may enhance the structure resistance to stability loss. These results open the door to further investigations aimed at uncovering mechanisms driving this phenomenon. Future analyses should focus on identifying the specific conditions that enable this increase in buckling resistance. This approach may also be beneficial for thin-walled plate structures, such as columns or girders, which are often subjected to complex loading and boundary conditions influenced by the interaction of adjacent walls.

APPENDIX A

The coefficients $a_1, a_2, \ldots, a_6$, from (A13)–(A18), $b_1, b_2, \ldots, b_6$ applied in (15)–(17) and (A13)–(A18), and $k_1, k_2, \ldots, k_6$ from (20) are defined as

$$a_1 = B_{11}^{**} + B_{22}^{**} - 2B_{66}^{**}, \tag{A1}$$

$$a_2 = -D_{12}^{*} - D_{21}^{*} - 4D_{66}^{*}, \tag{A2}$$

$$a_3 = B_{12}^{**}, \tag{A3}$$

$$a_4 = B_{21}^{**}, \tag{A4}$$

$$a_5 = D_{11}^{*}, \tag{A5}$$

$$a_6 = D_{22}^{*}, \tag{A6}$$

$$b_1 = 2A_{12}^{*} + A_{66}^{*}, \tag{A7}$$

$$b_2 = -B_{22}^{*} + 2B_{66}^{*} - B_{11}^{*}, \tag{A8}$$

$$b_3 = A_{22}^{*}, \tag{A9}$$

$$b_4 = A_{11}^{*}, \tag{A10}$$

$$b_5 = B_{21}^{*}, \tag{A11}$$

$$b_6 = B_{12}^{*}, \tag{A12}$$

$$k_1 = \pi^2 mn\,(a_3 b_4 + a_4 b_3) \cdot \frac{\left((-1)^m - 1 - (-1)^{m+n} + (-1)^n\right)}{6ba b_3 b_4}, \tag{A13}$$

$$k_2 = \frac{-\pi^4}{4a^3 b^3 \left(a^4 b_4 n^4 + a^2 b^2 b_1 m^2 n^2 + b^4 b_3 m^4\right)} \cdot \begin{pmatrix} n^8 \left(-a_4 b_6 + a_6 b_4\right) a^8 + n^6 b^2 m^2 \\ \cdot \left(-a_1 b_6 - a_2 b_4 + a_4 b_2 + a_6 b_1\right) a^6 \\ + b^4 m^4 n^4 \begin{pmatrix} a_1 b_2 - a_2 b_1 - a_3 b_6 \\ -a_4 b_5 + a_5 b_4 + a_6 b_3 \end{pmatrix} a^4 \\ + b^6 m^6 n^2 a^2 \\ \left(-a_1 b_5 - a_2 b_3 + a_3 b_2 + a_5 b_1\right) \\ + b^8 m^8 \left(-a_3 b_5 + a_5 b_3\right) \end{pmatrix}, \tag{A14}$$

$$k_3 = \frac{h\pi^2 bm^2}{4a}, \tag{A15}$$

$$k_4 = \frac{-\pi^4 \left(a^4 b_4 n^4 + b^4 b_3 m^4\right)}{64 b^3 a^3 b_3 b_4}, \tag{A16}$$

$$k_5 = 2n \left(a^4 b_6 n^4 - a^2 b^2 b_2 m^2 n^2 + b^4 b_5 m^4\right) \cdot \frac{m\pi^2 \left(-1 + (-1)^m\right)\left((-1)^n - 1\right)}{3ba \left(a^4 b_4 n^4 + a^2 b^2 b_1 m^2 n^2 + b^4 b_3 m^4\right)}, \tag{A17}$$

$$k_6 = hB_{11}^{**} mb \cdot \frac{\left(-(-1)^m + 1 + (-1)^{m+n} - (-1)^n\right)}{an} + h\left(RB_{22}^{**} + B_{21}^{**}\right) na \cdot \frac{\left(-(-1)^m + 1 + (-1)^{m+n} - (-1)^n\right)}{bm}. \tag{A18}$$

REFERENCES

[1] J.M. Hodgkinson, *Mechanical testing of advanced fibre composites*, Woodhead Publishing Ltd and CRC Press LLC, 2000.

[2] P.D. Mangalgiri, "Composite materials for aerospace applications," *Bull. Mater. Sci.*, vol. 22, no. 3, pp. 657–64, 1999.

[3] F.C. Campbell, *Manufacturing technology for aerospace structural materials*, 1st Ed., Elsevier Ltd, 2006, p. 616, doi: 10.1016/B978-1-85617-495-4.X5000-8.

[4] C.E. Harris, J.H. Starnes, and M.J. Shuart, "Design and manufacturing of aerospace composite structures, state-of-the-art assessment," *J. Aircr.*, vol. 39, pp. 545–560, 2002.

[5] J. Romanoff, H. Remes, P. Varsta, B.R. Goncalves, M. Korgesaar, and I. Lillemae-Avi, "Limit state analyses in design of thin-walled marine structures – Some aspect on length-scales," *J. Offshore Mech. Arct. Eng.*, vol. 142, no. 3, pp. 1–21, 2019, doi: 10.1115/1.4045371.

[6] R. Degenhardt, S.G.P. Castro, M.A. Arbelo, R. Zimmerman, R. Khakimova, and A. Kling, "Future structural stability design for composite space and airframe structures," *Thin-Walled Struct.*, vol. 81, pp. 29–38, 2014, doi: 10.1016/j.tws.2014.02.020.

[7] C.B. York, "Unified approach to the characterization of coupled composite laminates: Benchmark Configurations and special cases," *J. Aerosp. Eng.*, vol. 23, pp. 219–242, 2010, doi: 10.1061/(ASCE)AS.1943-5525.0000036.

[8] C.B. York, "On bending-twisting coupled laminates," *Compos. Struct.*, vol. 160, pp. 887–900, 2017, doi: 10.1016/j.compstruct.2016.10.063.

[9] C.B. York, "Laminate stiffness tailoring for improved buckling performance," *Thin-Walled Struct.*, vol. 161, p. 107482, 2021, doi: 10.1016/j.tws.2021.107482.

[10] Z. Kolakowski and R.J. Mania, "Influence of the coupling matrix B on the interactive buckling of FML-FGM columns with closed cross-sections under axial compression," *Compos. Struct.*, vol. 173, pp. 70–77, 2017, doi: 10.1016/j.compstruct.2017.03.108.

[11] A. Teter, R.J. Mania, and Z. Kolakowski, "Effect of selected elements of the coupling stiffness submatrix on the load-carrying capacity of hybrid columns under compression," *Compos. Struct.*, vol. 180, pp. 140–147, 2017, doi: 10.1016/j.compstruct.2017.08.001.

[12] T. Kubiak, M. Urbaniak, and F. Kazmierczyk, "The influence of the layer arrangement on the distortional post-buckling behaviour of open-section beams," *Materials*, vol. 13, p. 3002, 2002, doi: 10.3390/ma13133002.

[13] A. Teter and Z. Kolakowski, "Susceptibility versus flexural stiffness in the stability of hybrid laminate columns with a rectangular cross section for a 1D model," *Compos. Struct.*, vol. 345, no. 1, 118362, 2024, doi: 10.1016/j.compstruct.2024.118362.

[14] S. Samborski, "Analysis of the end-notched flexure test configuration applicability for mechanically coupled fiber reinforced composite laminates," *Compos. Struct.*, vol. 163, pp. 342–349, 2017, doi: 10.1016/j.compstruct.2016.12.051.

[15] S. Samborski, "Prediction of delamination front's advancement direction in the CFRP laminates with mechanical couplings subjected to different fracture toughness tests," *Compos. Struct.*, vol. 202, pp. 643–650, 2018, doi: 10.1016/j.compstruct.2018.03.045.

[16] D. Cui and D. Li, "Bending-twisting coupled structures based on composite laminates with extension-shear coupling effect," *Compos. Struct.*, vol. 209, pp. 434–442, 2019, doi: 10.1016/j.compstruct.2018.09.095.

[17] Q. Ansari, G. Zucco, L.C. Trinh, and P.M. Weaver, "Compression buckling of elastically supported cylindrical shells with Bend/Twist coupling," *Compos. Struct.*, vol. 309, p. 116691, 2023, doi: 10.1016/j.compstruct.2023.116691.

[18] J. Loughlan, "The influence of mechanical couplings on the compressive stability of antisymmetric angle-ply laminates," *Compos. Struct.*, vol. 57, pp. 473–482, 2002, doi: 10.1016/S0263-8223(02)00116-2.

[19] K. Falkowicz, S. Samborski, and P.S. Valvo, "Effects of Elastic Couplings in a Compressed Plate Element with Cutout," *Materials*, vol. 15, 7752, 2022, doi: 10.3390/ma15217752.

[20] K. Falkowicz, "Validation of extension-bending and extension-twisting coupled laminates in elastic element," *Adv. Sci. Technol. Res. J.*, vol. 17, no. 3, pp. 309–319, 2023, doi: 10.12913/22998624/167451.

[21] M. Bohlooly Fotovat, and T. Kubiak, "Non-bifurcation behavior of laminated composite plates under in-plane compression," *Bull. Pol. Acad. Sci. Tech. Sci.*, vol. 72, no. 2, p. e148874, 2024, doi: 10.24425/bpasts.2024.148874.

[22] B.D. Davidson and R.A. Schapery, "A technique for predicting mode I energy release rates using a first-order shear deformable plate theory," *Eng. Frac. Mech.*, vol. 36, pp. 157–165, 1990, doi: 10.1016/0013-7944(90)90105-P.

[23] M.P. Nemeth, "Importance of anisotropy on buckling of compression loaded symmetric composite plates," *AIAA J.*, vol. 24, no. 11, pp. 1831–1835, 1986.

[24] P. Weaver and M.P. Nemeth, "Bounds on flexural properties and buckling response for symmetrically laminated composite plates," *J. Eng. Mech.*, vol. 133, pp. 1178–1191, 2007, doi: 10.1061/(ASCE)0733-9399(2007)133:11(1178).

[25] R.M. Jones, *Mechanics of Composite Materials*, 2nd ed.; CRC Press: Boca Raton, FL, USA, 2018.

[26] A.T. Nettles, *Basic mechanics of laminated composite plates*. NASA reference publication, 1994, p. 107.

[27] User's Guide ANSYS® R1, Ansys, Inc.: Canonsburg, USA, 2023.

[28] J. Singer, J. Arbocz, and T. Weller, "Buckling Experiments: Experimental Methods" in *Buckling of Thin-Walled Structures: Basic Concepts, Columns, Beams and Plates*, John Wiley & Sons Inc., 2000, doi: 10.1002/9780470172988.

[29] M. Paszkiewicz and T. Kubiak, "Selected problems concerning determination of the buckling load of channel section beams and columns," *Thin-Walled Struct.*, vol. 93, pp. 112–121, 2015, doi: 10.1016/j.tws.2015.03.009.

[30] M. Zaczynska and Z. Kołakowski, "The influence of the internal forces of the buckling modes on the load-carrying capacity of composite medium-length beams under bending," *Materials*, vol. 13, p. 455, 2020, doi: 10.3390/ma13020455.